Local Synergetic Collaboration between Pd and local tetrahedral symmetric Ni Oxide enables ultra-high-performance CO_2 Thermal Methanation

Authors: Che Yan,[a] Chia-Hsin Wang,[b*] Moore Lin,[c] Dinesh Bhalothia,[a] Shou-Shiun Yang,[a] Gang-Jei Fan,[c] Jia-Lin Wang,[c] Ting-Shan Chan,[b] Yao-lin Wang,[d] Xin Tu,[d] Sheng Dai,[e] Kuan-Wen Wang,[f] Jr-Hau He,[g] and Tsan-Yao Chen[a, h, i*]

Affiliations:

[a] Department of Engineering and System Science, National Tsing Hua University, Hsinchu 30013, Taiwan

[b] National Synchrotron Radiation Research Center, Hsinchu 30076, Taiwan

[c] Department of Chemistry, National Central University, Taoyuan 32001, Taiwan

[d] Department of Electrical Engineering and Electronics, University of Liverpool, Liverpool L69 3GJ, UK

[e] School of Chemistry & Molecular Engineering, East China University of Science and Technology, Shanghai 200237, P.R. China

[f] Institute of Materials Science and Engineering, National Central University, Taoyuan City 32001, Taiwan.

[g] Department of Materials Science and Engineering, City University of Hong Kong, Hong Kong

[h] Institute of Nuclear Engineering and Science, National Tsing Hua University, Hsinchu 30013, Taiwan

[i] Hierarchical Green-Energy Materials (Hi-GEM) Research Centre, National Cheng Kung University, Tainan 70101, Taiwan

Corresponding Authors:

Chia-Hsin Wang

Email: wang.ch@nsrrc.org.tw

Tel: +886-3-5780281 # 7327

FAX: +886-3-5783813

Tsan-Yao Chen

Email: chencaeser@gmail.com

Tel: +886-3-5715131 # 34271

FAX: +885-3-5720724

1. Benchmark for the CO_2RR performances of bimetallic and multi-metallic nanocatalysts

Catalytic transformation of CO_2 into methane (CH_4) via heterogenous nanocatalysts is an effective approach to overcome the longstanding dilemma of energy crisis and serious increment of CO_2 concentration in atmosphere. Some of recent advancements in the design of heterogeneous nanocatalysts towards CO_2 methanation are summarized in **Table S1**. Accordingly, most bi- and multi-metallic heterogenous NCs possesses an optimum CH_4 production yield nearly around 300-600 µmol/$g_{catalyst}$ in a reaction gas of a low CO_2 concentration around 7-25%. For Ni-based NCs, reduced Ni and oxygen vacancies are found the most preferential sites for CO_2 adsorption, however, the formation of di- or tri-carbonyls and/or stable polycarbonates block the CO_2 adsorption sites resulting into the deactivation of Ni-based catalyst.[1-3] On the other hand for Ru-based NCs, intermediate carbonyl species at the metal– support interface and metal interface leads to decomposition of NCs and thus comes out with relatively suppressed catalytic performance.[4-5] Moreover, the nature and population of intermediate species depend strongly on composition and reaction temperature of feeding gases, which are cardinal performance determining factors for ultimate production yield for CH_4. To overcome the aforementioned bottlenecks, we demonstrate the unique synergetic collaborations between local tetrahedral symmetric NiO_T and metallic Pd-nanocrystal in interface can significantly promotes the CO_2 methanation as compared to that of previously reported studies (**Table S1**). In such a unique NC, Ni-oxide (i.e. NiO_T) is reduced to metallic form by interacting with H_2 and the local synergetic collaboration between metallic Ni sites (the chemisorbed H in Ni, Ni*-H^{ads}) and Pd sites (the chemisorbed CO in Pd, Pd*-CO^{ads}) in the Pd-to-NiO_T interface triggers the methanation reaction at near room temperature (consistently proved by the in-situ ambient pressure XPS).

Table S1 Benchmark for the CO₂RR performances of bimetallic and multi-metallic nanocatalysts

Catalyst Support	Metal contents	Temperature (°C)	Feeding gas	S_{CH4} (%)*	Yield$_{CH4}$ (μmol/g)	References
MWCNT	NiPd-TMOS (NiO$_T$Pd-T)	~300	CO_2: H_2 = 1: 3	N/A	1905.1	This work
	NiO$_T$-T				1083.2	
	Pd-T				92.2	
Al$_2$O$_3$	0.1% Pd, 10%Ni, 6.1% "Na$_2$O"	500	7.5% CO_2, 15% H_2/N_2	N/A	180.0	1
	0.1% Pt, 10%Ni, 6.1% "Na$_2$O"				160.0	
	1% Pt, 10%Ni, 6.1% "Na$_2$O"				250.0	
	Ru15%CaO	400	1.4% CO_2+ 10% H_2	N/A	414.0	21
	1% Ru, 10% Ni, 6.1% "Na$_2$O"	320	7.5% CO_2, 15% H_2/N_2	~100	380.0	1
	Ru10%Na$_2$CO$_3$	310	1.4% CO_2+ 10% H_2	N/A	383.0	21
	5 wt.% Ni/2 wt.% ceria	300		100		2
	20 wt.% Ni/H	300		>99		2
ZrO$_2$	2CA-Co/ZrO$_2$	400		99		10
SiO$_2$	Ni/SiOx-2	400		91.4		13
	Ni/SiO$_2$	250		~100		2
CeO$_2$	10 wt% Ni/CeO$_2$	350	CO_2: H_2 = 1: 4	100		2
	25Ni-20CeO$_2$	300		100		12
TiO$_2$	15 wt% Ni/TiO$_2$	260		99	N/A	2
Alloys and Compounds	15 wt% Ni–La/SiC	360		100		2
	10 wt% Ni/β-zeolite	360		N/A		2
	5 wt% Ni–Ce$_x$Zr$_{1−x}$O$_2$	350		>98		2
	5 wt% Ni/ceria zirconia	350		98.4		2
	Ru-SA	310		99.5		8
	70 wt% Ni/SBA-15	300	CO_2: H_2 = 1: 7	100		2
	10 wt% Ni/β-zeolitewith plasma	240	CO_2: H_2 = 1: 3	N/A		2
	35 wt% Ni/5 wt% Fe/ Alumina xerogel	220	CO_2: H_2: N2 = 1: 4: 1.7	99.5		2
	NiMn(1:2)	200	CO_2: H_2 = 1: 4	99.6		14

*S_{CH4} (%) represents the selectivity of CO_2 methanation (i.e. the conversion rate of inlet CO_2 to CH_4). Whereas, in the present study the optimum production yield has been reported instead of conversion efficiency.

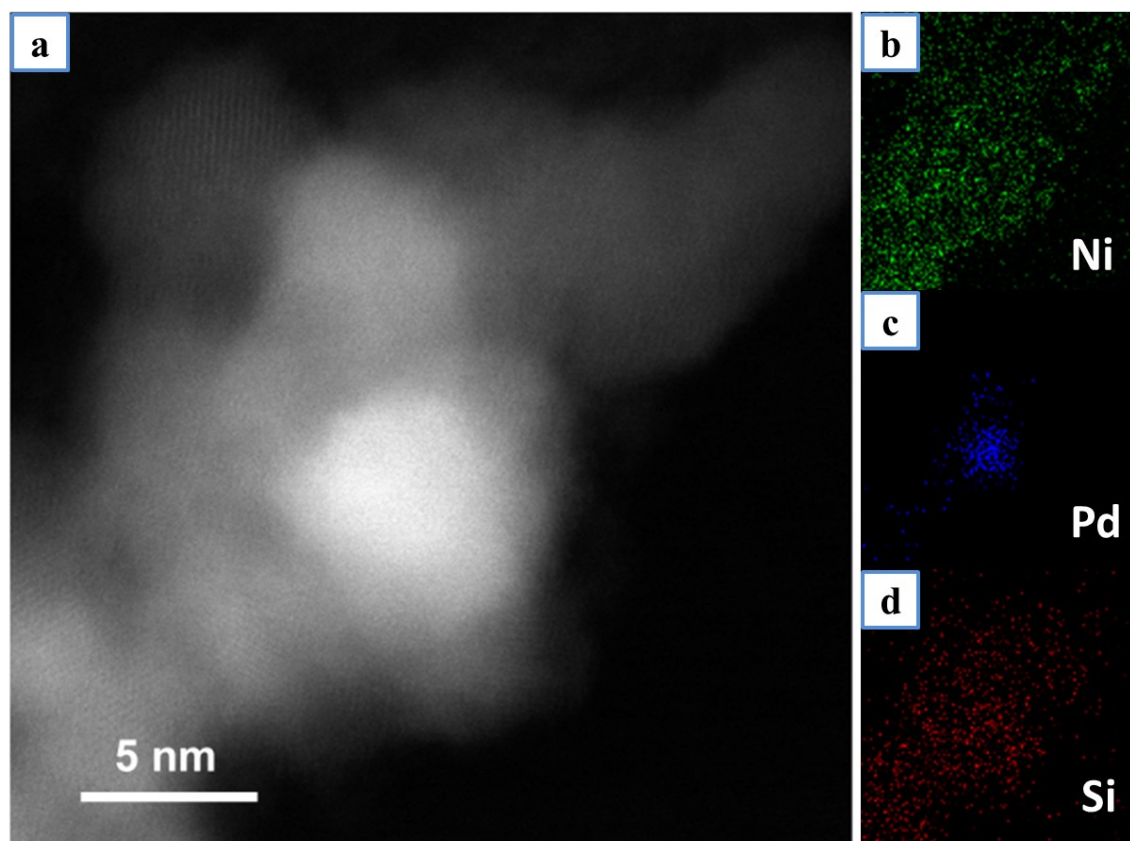2. HRTEM inspections on the crystal structure of NiO_TPd-T and Pd-T

Figure S1 Scanning transmission electron microscopy (STEM) of heterogeneous Pd nano-islands grown onto NiO_T NCs with chemisorbed TMOS layer. **a** HAADF-STEM image of NiO_TPd-T. **b–d** EDS elemental mapping of the NiO_TPd-T in **a**.
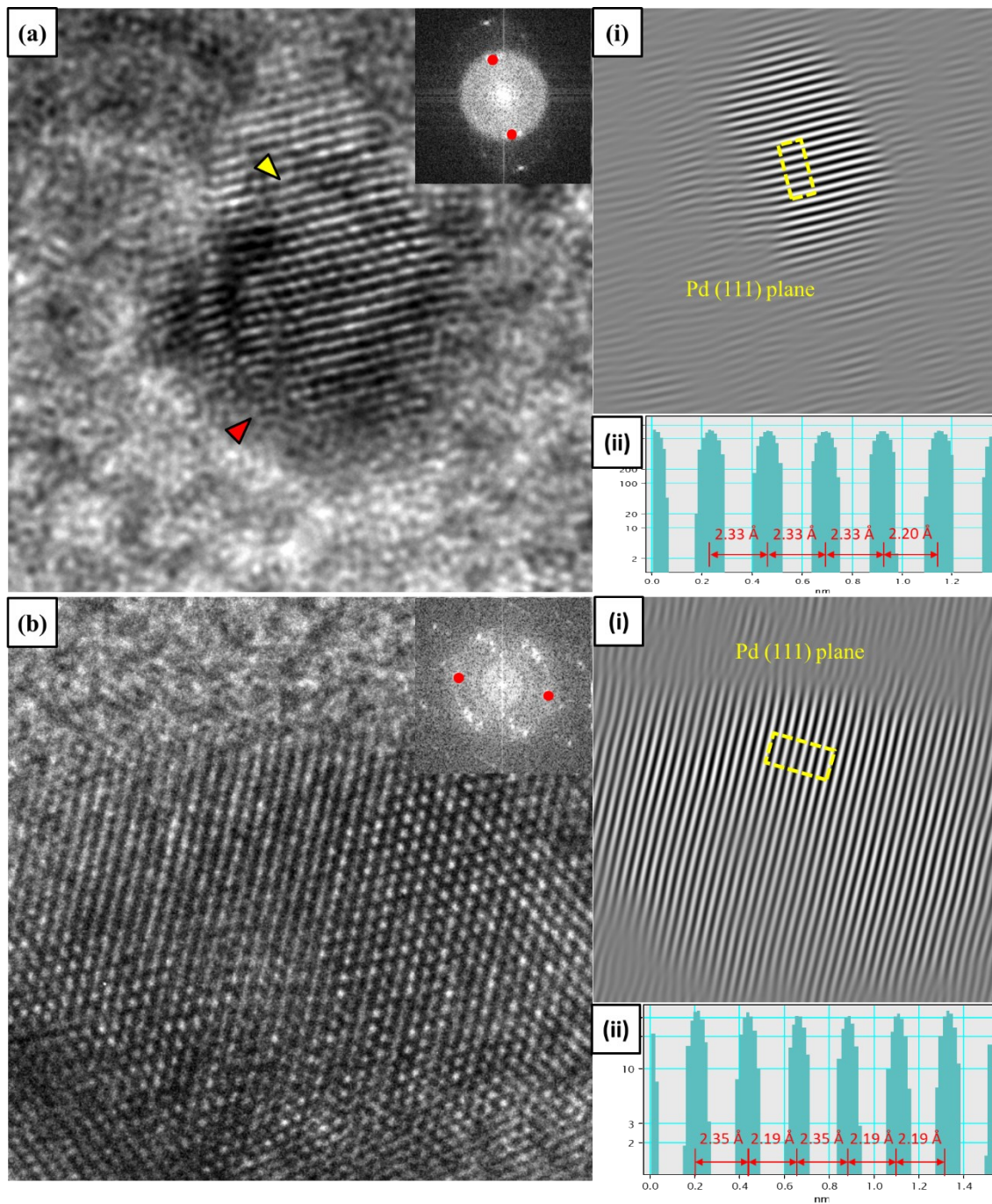
Figure S2 HRTEM images of **a** NiO$_T$Pd-T and **b** Pd-T. The Fourier transformation pattern, the Forward Fourier Transformation image of the image, and the corresponding line histogram in the selected region (dashed rectangular) along (111) facet are respectively shown in the inset, (i), and (ii).
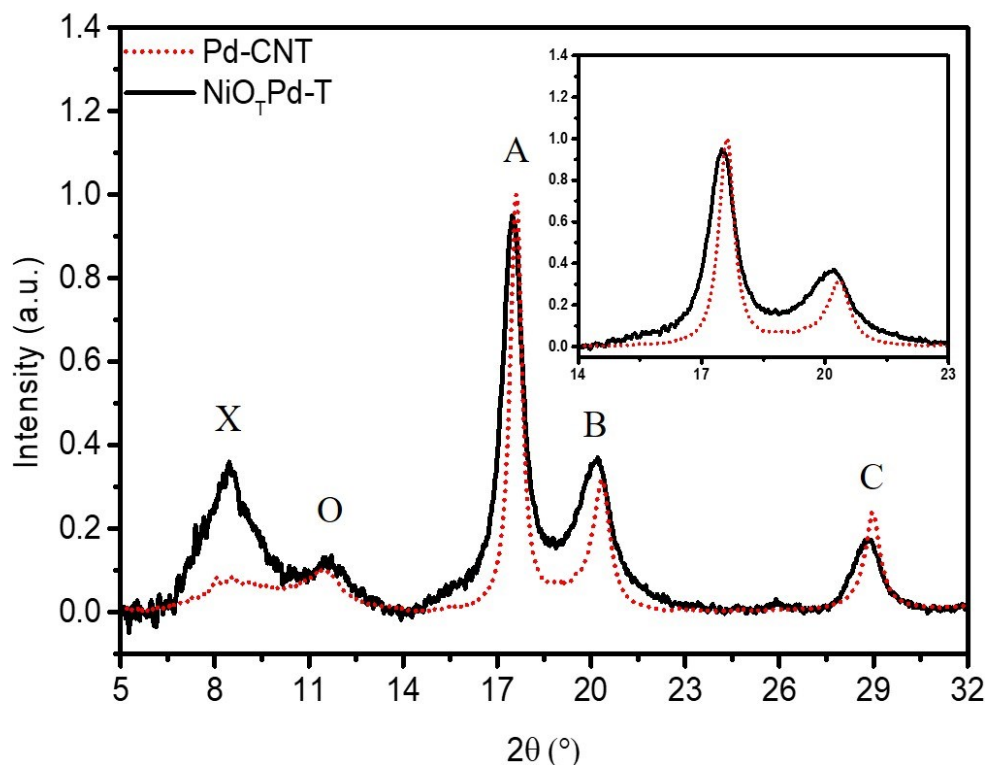
3. X-ray diffraction analysis

Figure S3 X-ray diffraction pattern of the control sample (Pd/A-CNT, red) and experimental sample (NiO$_T$Pd-T, black) NCs. X and O denote NiO$_2$ (111) and CNT (002) plane, respectively. A, B, and C denote Pd (111), (200) and (220) plane, respectively. Inlet pattern zooms in the 2θ range from 15˚ to 22˚.

Table S2 Parameters of d-spacing and grain size from X-ray diffraction (111) and (200) planes for Pd/A-CNT and NiO$_T$Pd-T NCs.

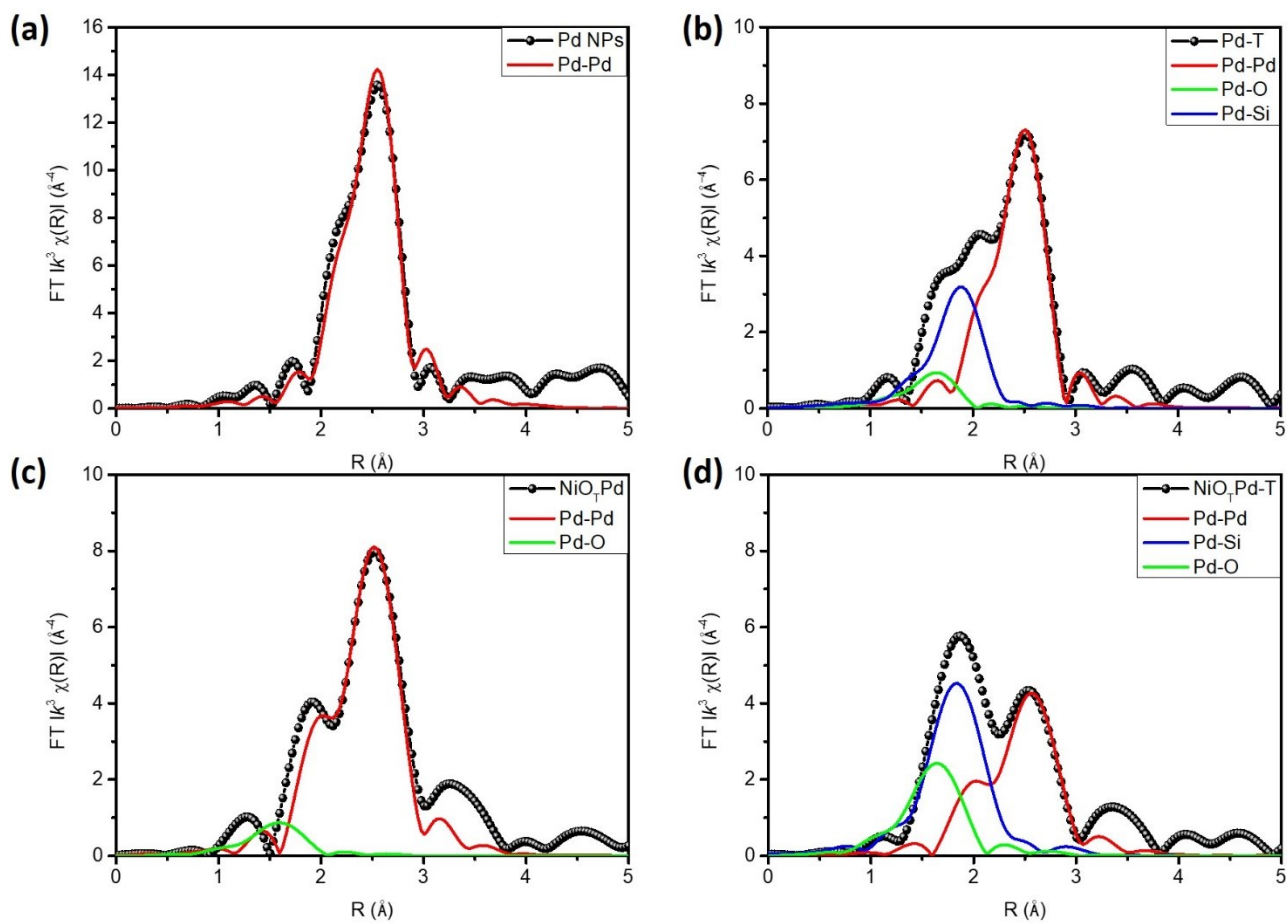| sample	d$_{(111)}$ (Å)	d$_{(200)}$ (Å)	d$_{(220)}$ (Å)	D$_{(111)}$ (nm)	D$_{(200)}$ (nm)	D$_{(200)}$ (nm)
Pd/A-CNT	2.250	1.954	1.377	8.25	5.17	5.06
NiO$_T$Pd-T	2.265	1.974	1.385	4.92	2.42	3.46

4. Pd and Ni K-edge XAS analysis

Figure S4. Model analysis fitting curves compared with experimental FT-EXAFS spectra at Pd k-edge of (a) Pd, (b) Pd-T, (c) $NiO_T Pd$ and (d) $NiO_T Pd$-T.

Table S3 XAS model analysis determined local structure parameters of Pd-T and NiO$_T$Pd-T with control samples

NCs	Bond pair	CN	R (Å)
Pd	Pd-Pd	8.09	2.756
	Pd-Si	0	0
	Pd-O	0	0
Pd-T	Pd-Pd	4.62	2.762
	Pd-Si	2.17	2.367
	Pd-O	0.89	2.137
NiO$_T$Pd	Pd-Pd	6.81	2.746
	Pd-Si	0	0
	Pd-O	0.91	2.125
	Pd-Pd	3.91	2.781
NiO$_T$Pd-T	Pd-Si	3.47	2.361
	Pd-O	2.72	2.177
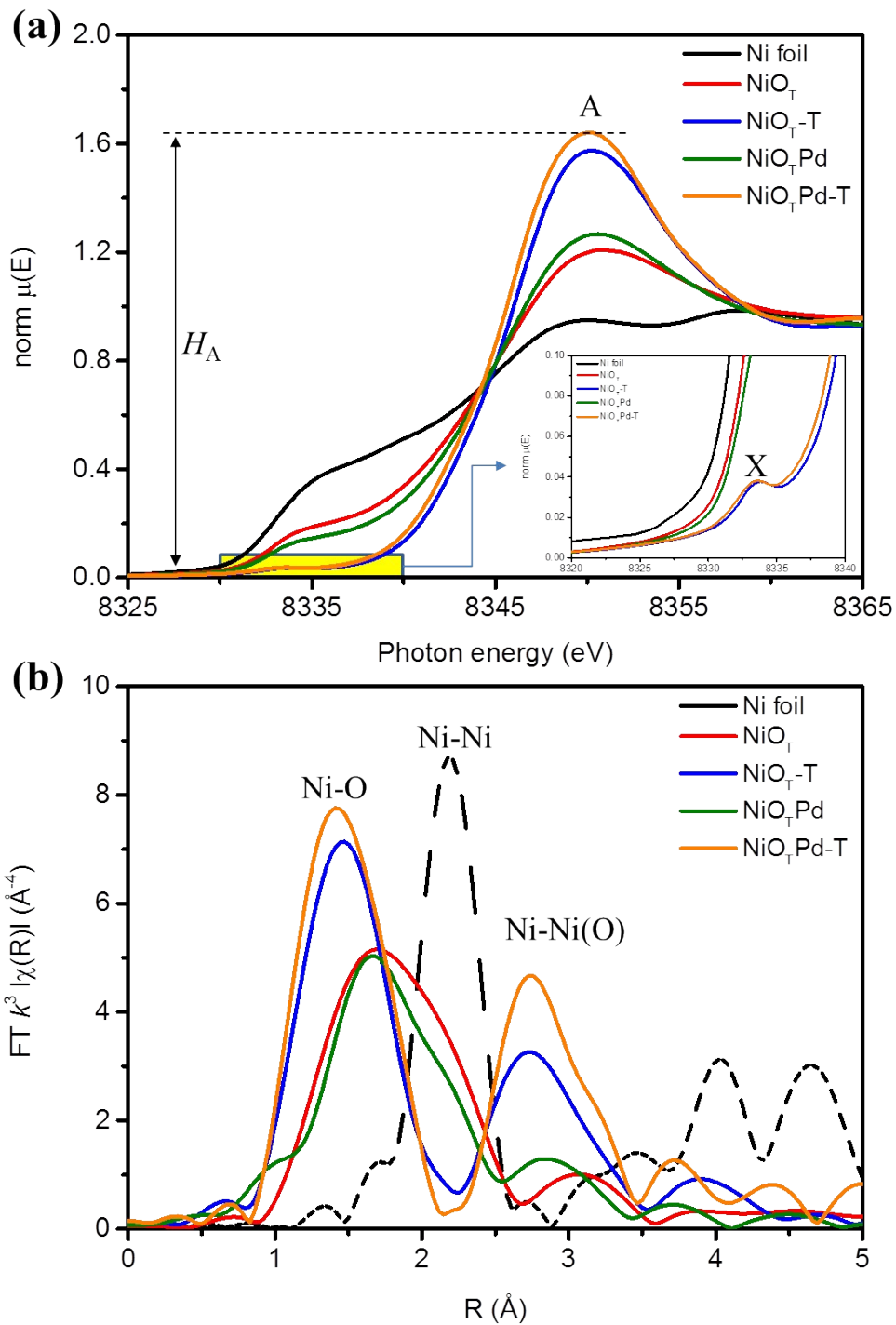
Figure S5 (**a**) X-ray absorption near-edge spectra (XANES) and (**b**) Fourier-transformed extended X-ray absorption fine structure (FT-EXAFS) for NiO_TPd-T and control samples (Ni foil, NiO_T, NiO_T-T, and NiO_TPd NPs) at Ni K-edge. Inset of **Figure S5a** zooms in the pre-edge region (X) of XANES spectra.

5. Performance of control and experimental samples

Table S4 Calibrated product concentration of CO and CH_4 under 0.11 mbar CO_2 and mixing (CO_2+H_2) atmospheres from 323 K to 573 K for 12 mg of the control samples (NiO_T-T and Pd-T) and the experimental sample (NiO_TPd-T).

Sample	NiO_T-T				Pd-T				NiO_TPd-T			
Feeding gas	CO_2		CO_2+H_2		CO_2		CO_2+H_2		CO_2		CO_2+H_2	
Temp. (K) / Products*	CO	CH_4	CO	CH_4	CO	CH_4	CO	CH_4	CO	CH_4	CO	CH_4
323	N/A	N/A	N/A	N/A	N/A	N/A	N/A	N/A	N/A	0.2	N/A	0.5
373	N/A	N/A	N/A	N/A	N/A	N/A	N/A	8.2	N/A	0.9	N/A	4.1
423	N/A	N/A		0.5	N/A	0.4	N/A	25.2	N/A	1.5	44.8	18.3
473	N/A	N/A	7.1	12.3	33.7	0.6	N/A	86.5	73.2	1.9	241.5	110.3
523	N/A	N/A	245.3	187.7	54.8	0.8	147.3	27.2	334.4	3.3	1208.2	530.6
573	11.8	N/A	2272.3	1083.2	87.5	1.5	636.8	92.2	852.6	2.7	3629.5	1905.0

*The unit of the concentration is µmol/$g_{catalyst}$.

Table S5 Calibrated product concentration of CO and CH_4 under 0.11 mbar CO_2 and mixing (CO_2+H_2) atmospheres from 323 K to 573 K for 12 mg of the control samples (NiO_T-T and Pd-T) and the experimental sample (NiO_TPd-T).

Sample	NiO_T-T				Pd-T				NiO_TPd-T			
Feeding gas	CO_2		CO_2+H_2		CO_2		CO_2+H_2		CO_2		CO_2+H_2	
Temp. (K) / Products*	CO	CH_4	CO	CH_4	CO	CH_4	CO	CH_4	CO	CH_4	CO	CH_4
323	N/A	N/A	N/A	N/A	N/A	N/A	N/A	N/A	N/A	3.2	N/A	8.0
373	N/A	N/A	N/A	N/A	N/A	N/A	N/A	131.2	N/A	14.4	N/A	65.6
423	N/A	N/A		8.0	N/A	6.4	N/A	403.2	N/A	24.0	44.8	292.8
473	N/A	N/A	113.6	196.8	539.2	9.6	N/A	1384.0	1171.2	30.4	3864.0	1764.8
523	N/A	N/A	3924.8	3003.2	876.8	12.8	2356.8	435.2	5350.4	52.8	19331.2	8489.6
573	188.8	N/A	36356.8	17331.2	1400.0	24.0	10188.8	1475.2	13641.6	43.2	58072.0	30480.0

* The unit of the concentration is µg/$g_{catalyst}$.

6. CO$_2$RR mechanisms on NiO$_T$-T NCs

Table S6. The proposed reaction coordinates and the corresponding coordination loop for the control sample NiO$_T$-T on CO$_2$RR.

| No.	reaction coordinates	intermediate species	subsequent reaction	intermediate species	subsequent reaction	Product
(1)	Ni^{d}* + H$_2$ → Ni*-H$_2$^{ads}	Ni*-H$_2$^{ads}	(2)			
(2)	Ni*-H$_2$^{ads} + Ni^{d}* → 2Ni*-H^{ads}	Ni*-H^{ads}	(3)			
(3)	Ni-O + Ni*-H^{ads} → Ni*-OH^{ads} + Ni^0*	Ni*-OH^{ads}	(4)	Ni^0*	(5) (8)	
(4)	Ni*-OH^{ads} + Ni*-H^{ads} → Ni*-H$_2$O^{ads} + Ni^0* → Ni^0* + H$_2$O$_{(g)}$	Ni^0*	(5) (8)			H$_2$O
(5)	Ni^0* + CO$_2$ → Ni*-CO$_2$^{ads}	Ni*-CO$_2$^{ads}	(6)			
(6)	Ni*-CO$_2$^{ads} + Ni^0* → Ni*-CO^{ads} + Ni*-O^{ads}	Ni*-CO^{ads}	(10)	Ni*-O^{ads}	(9)	
(7)	Ni*-CO^{ads} → Ni^0* + CO$_{(g)}$	Ni^0*	(5) (8)			CO
(8)	2Ni^0* + H$_2$ → 2Ni*-H^{ads}	Ni*-H^{ads}	(3)			
(9)	Ni*-O^{ads} + Ni*-H^{ads} → Ni*-OH^{ads} + Ni^0*	Ni*-OH^{ads}	(4)	Ni^0*	(5) (8)	
(10)	Ni*-CO^{ads} + Ni*-OH^{ads} → Ni*-COH^{ads} + Ni*-O^{ads}	Ni*-COH^{ads}	(11)	Ni*-O^{ads}	(9)	
(11)	Ni*-COH^{ads} + Ni*-H^{ads} → Ni*-CH$_2$^{ads} + Ni*-O^{ads}	Ni*-CH$_2$^{ads}	(12)	Ni*-O^{ads}	(9)	
(12)	Ni*-CH$_2$^{ads} + 2Ni*-H^{ads} → Ni*-CH$_4$^{ads} + 2Ni^0* → Ni^0* + CH$_{4(g)}$	Ni^0*	(5) (8)			CH$_4$

7. GC system
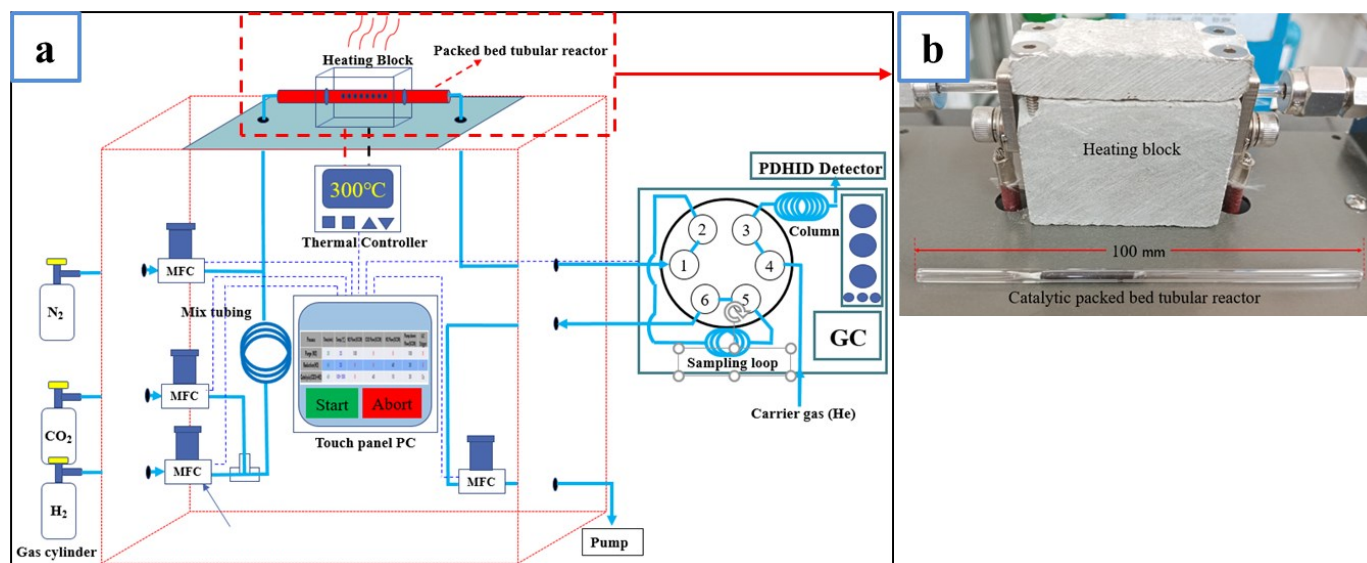
Figure S6 Schematic diagram of (a) the experimental apparatus for an automatic premixed gas supply equipped with a catalyst-packed thermal reaction bed. (b) the catalyst reaction bed by pacing a chosen catalyst into a glass tube. The tube is enclosed within a heating block.
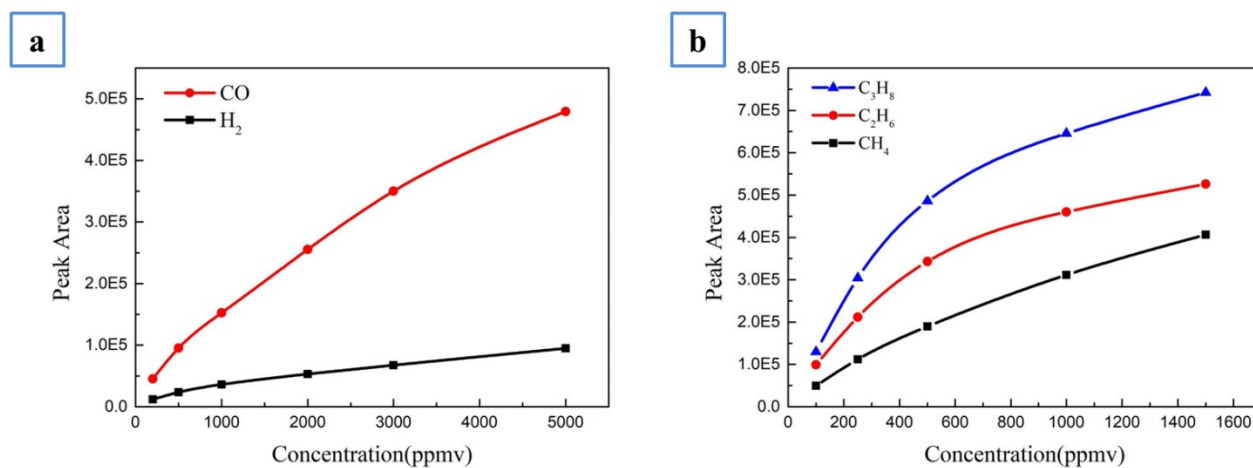

Figure S7 Calibration curves for (a) hydrogen and carbon monoxide, (b) methane, ethane, and propane.

Table S7 Repeatability of selected gases.

Gas type	Repeatability (%RSD)*
H_2	0.82
CO	0.27
CH_4	0.22
C_2H_6	0.16
C_3H_8	0.22

8. Calculation Details for CH_4 production yield.

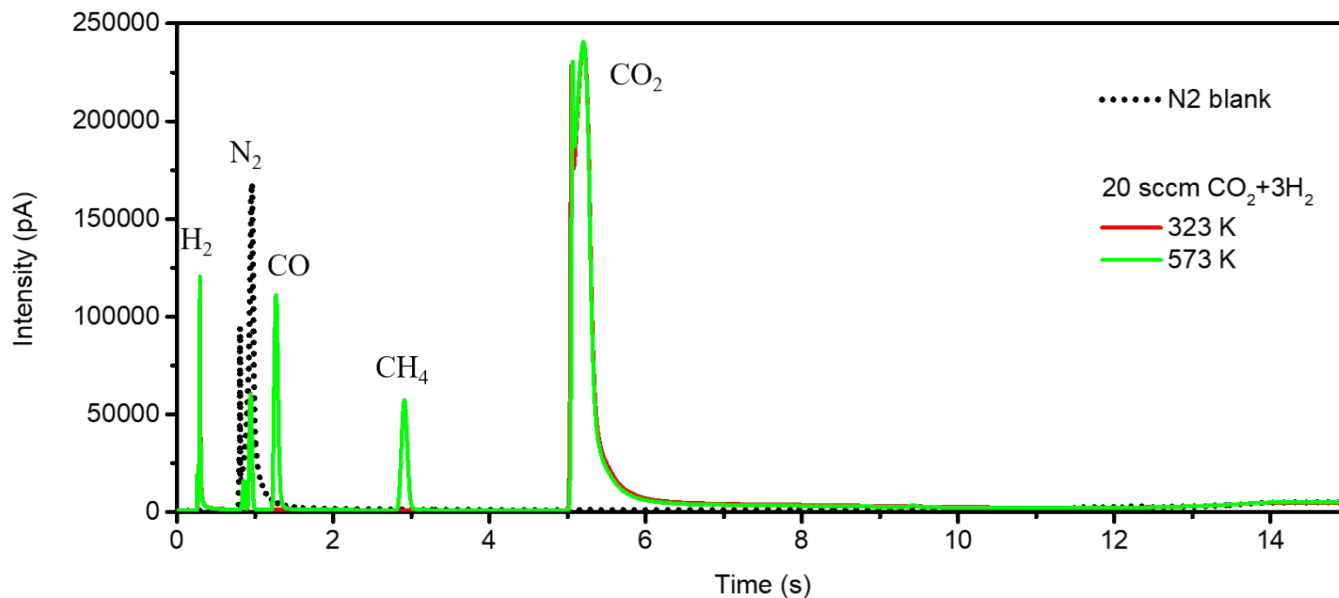1. Got the full-scale GC curve as in **Figure R4**

Figure S8. Full scale of GC curves.

2. Integrate the peak area for all peaks (CH_4 peak in this case), as shown in **Figure S9**.
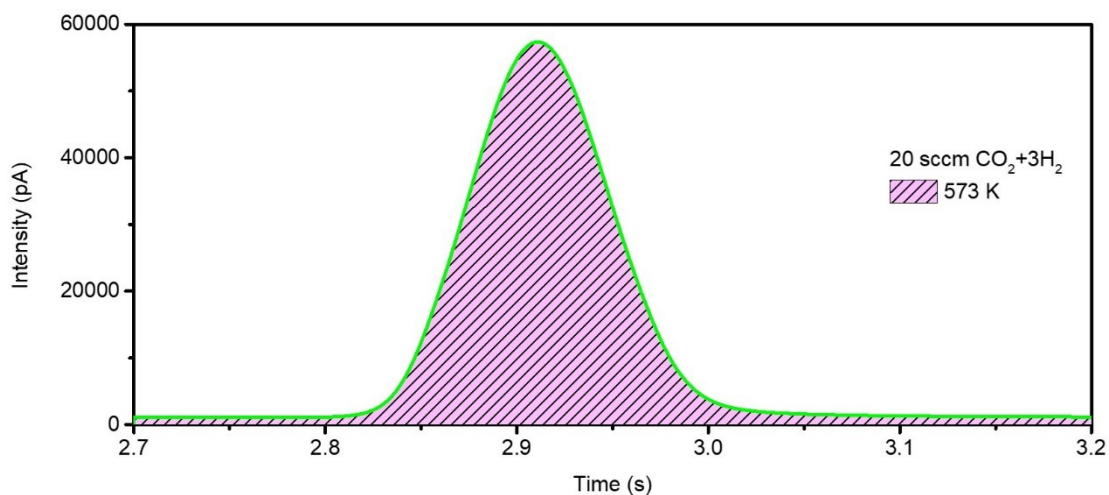

Figure S9. The integrated area of CH_4 peak.

3. The integrated area of CH_4 peak is 298738 pA.

4. The integrated area of CH_4 peak (Experimental sample) is divided by the integrated area of CH_4 peak (Pure CH_4 gas in a 20 sccm flow rate) and times the concentration of CH_4 (29.9 ppmv marked on gas bottle). ------ Eq. 1

5. Transform the unit of ppmv to μg: ppmv is divided by the volume (in normal temperature and pressure condition, i.e. 24.45 liter) and times the molecular weight. ------Eq. 2

$$CH_4\ (\mu g) = CH_4 \div 24.45\ (mole) \times M.W. \frac{g}{(mole)} \frac{\mu g}{(g)} \text{------- Eq. 2}$$

$$365.328\ (\mu g) = 558.267 \div 24.45\ (mole) \times 16.0 \frac{g}{(mole)} \frac{\mu g}{(g)}$$

6. Transform from μg to μmol: μg is divided by molecular weight. ------Eq. 3

7. Finally, μmol is divided by the weight of catalyst (g). ------Eq. 4

$$\frac{CH4\ (\mu mol)}{\text{gram of catalyst}} = \frac{22.833}{12\ mg \times 0.001} = 1902.8 \frac{\mu mol}{g} \text{------- Eq. 4}$$

A complete derivation process is showed below:

- P is the pressure of the gas (in atm),
- V is the volume of the gas (in liter),
- n is the amount of substance of gas (also known as number of moles),
- W is the total mass of the gas (in grams),
- M is the molar mass (in grams per mole),
- R is the ideal, or universal, gas constant, equal to the product of the Boltzmann constant and the Avogadro constant (0.0821 liter $\times$ atm/mole $\times$ K),
- T is the absolute temperature of the gas (in K).

In normal temperature and pressure condition (NTP), P = 1 atm, T = 298 K. Assume that the concentration of CH_4 is dilute, that is, in ppmv level compared with air and equals to X ppmv (Parts per million by volume in Air, ppmv = $\frac{1\ gas\ volume}{10^6\ air\ volume}$).

$$PV = \frac{W}{M} RT, (n = \frac{W}{M}), \text{ideal gas equation}$$

$$\rightarrow W = \frac{PV}{RT} M$$

According to the ideal gas equation, if there is one mole of air, the volume of air, V_{air}, is $\frac{RT}{P} = $ $\frac{0.0821\ (\frac{atm\ \times\ liter}{mole\ \times\ K}) \times 298\ (K)}{1\ (atm)}$ = 24.45 liter/mole and the concentration of CH_4, X, can be obtained from $\frac{V}{V_{air}}$. Then,

$$W = \frac{V}{V_{air}} M$$

15

$$\rightarrow W\ (g) = X\ (ppmv)\ \frac{1}{24.45}\ (mole)\ M\ (\frac{g}{mole})$$

The right hand side times 10^6 to transform from g to μg.

$$W\ (\mu g) = X\ (ppmv)\ \frac{1}{24.45}\ (mole)\ M\ (\frac{g}{mole})\ \times\ 10^6\ (\frac{\mu g}{g})$$

$$\rightarrow CH_4\ (\mu g) = CH_4\ (ppmv)\ \times \frac{1}{24.45}\ (mole) \times\ \frac{g}{M.W.\ (mole)}\ \times\ 10^6\ (\frac{\mu g}{g})$$

Expand the ppmv to 10^{-6} and rearrange the formula as Eq.2.

$$CH_4\ (\mu g) = CH_4\ \times\ 10^{-6}\ \times \frac{1}{24.45}\ (mole) \times\ M.W.\ (\frac{g}{mole}) \times\ 10^6\ (\frac{\mu g}{g})$$

$$CH_4\ (\mu g) = CH_4\ \div\ 24.45\ (mole)\ \times\ M.W\ (\frac{g}{mole})\ (\frac{\mu g}{g})\ \text{------- Eq. 2}$$

References

1. P. A. U. Aldana, F. Ocampo, K. Kobl, B. Louis, F. ThibaultStarzyk, M. Daturi, P. Bazin, S. Thomas and A. C. Roger, *Catal. Today*, 2013, **215**, 201.
2. Q. Pan, J. Peng, S. Wang and S. Wang, *Catal. Sci. Technol.*, 2014, **4**, 502.
3. M. A. A. Aziz, A. A. Jalil, S. Triwahyono and S. M. Sidik, *Appl. Catal.*, A, 2014, **486**, 115
4. S. Akamaru, T. Shimazaki, M. Kubo and T. Abe, *Appl. Catal.*, A, 2014, **470**, 405
5. P. Panagiotopoulou, D. I. Kondarides and X. E. Verykios, Catal. *Today*, 2012, **181**, 138.